

## Recent Advances in Silicon Photonic Integrated Circuits

John E. Bowers\*, Tin Komljenovic, Michael Davenport, Jared Hulme, Alan Y. Liu, Christos T. Santis, Alexander Spott, Sudharsanan Srinivasan, Eric J. Stanton, Chong Zhang  
Department of Electrical and Computer Engineering, University of California,  
Santa Barbara, CA 93106, USA  
\*bowers@ece.ucsb.edu

### ABSTRACT

We review recent breakthroughs in silicon photonics technology and components and describe progress in silicon photonic integrated circuits. Heterogeneous silicon photonics has recently demonstrated performance that significantly outperforms native III-V components. The impact active silicon photonic integrated circuits could have on interconnects, telecommunications, sensors and silicon electronics is reviewed.

**Keywords:** Heterogeneous silicon platform, integrated optoelectronics, optoelectronic devices, semiconductor lasers, silicon-on-insulator (SOI) technology, silicon photonics

### 1. INTRODUCTION

Heterogeneous silicon photonics, due to its potential for medium- and large-scale integration, has been intensively researched. Recent developments have shown that heterogeneous integration not only allows for a reduced cost due to economy of scale, but also allows for same or even better performing devices than what has previously been demonstrated utilizing only III-V materials. Furthermore we believe that optical interconnects are the only way to solve the scaling limitation in modern processors, and that heterogeneous silicon photonics with on-chip sources is the best approach in the long term as it promises higher efficiency and lower cost. We address both beliefs in sections that follow.

In this paper we plan to briefly address heterogeneous silicon approaches, and point-out that the heterogeneous silicon platform is more than just III-V on silicon but can have advantages for isolators, circulators and nonlinear devices (Section 2). We then present a short rationale on answering the question of why to use heterogeneous silicon photonics for interconnects (Section 3). We address passives (Section 4), outlining low-propagation loss and tight confinement benefits for integration, briefly touch upon polarization control on-chip as it is crucial for many new applications including polarization-diversity transceivers (Section 4.1) and we address tuning and temperature stability (Section 4.2). After passives, we highlight some recent record-performing active devices (Section 5) and provide a brief overview of sensors-on-chip progress (Section 5.1). We address narrow-linewidth lasers in general (Section 6) and then present record results together with theoretical explanations for record breaking results; first for single-wavelength lasers (Section 6.1) and then for widely-tunable ones (Section 6.2), finally we predict that sub-kHz linewidths should be possible with low-loss waveguide platform (Section 6.3).

We give special attention to narrow-linewidth lasers, as we believe that this is one of the areas that perfectly demonstrates the potential and benefits of utilizing heterogeneous approaches as recent performance of heterogeneously integrated narrow-linewidth lasers has far surpassed linewidth results demonstrated with III-V semiconductor lasers. Another area where this platform clearly shows its advantage are heterogeneously integrated high-power, high-speed photodiodes. We should point out that, due to the vast scope of research in this area and the high volume of publications, this paper, although covering a wide range of heterogeneous silicon photonics, will not provide an exhaustive list of published papers in the field.

### 2. HETEROGENEOUS SILICON PHOTONICS

One of the main motivations behind silicon photonics lies in its potential for bringing the large wafer size, volume throughput, and cost reduction of silicon manufacturing to photonic components. The silicon-on-insulator (SOI) platform fabrication infrastructure is compatible with CMOS technology and is highly accurate and mature, leading to a robust, high yield and reproducible technology. Photonic integrated circuits (PICs) operating in the telecommunication windows

around wavelengths of 1.3 and 1.55  $\mu\text{m}$  are perfect candidates for the SOI platform, which offers excellent waveguide capabilities as described in Section 4 about passive components. Prime applications for SOI-based PICs are telecommunications, interconnects, and lately sensors or sensor-systems on chip.

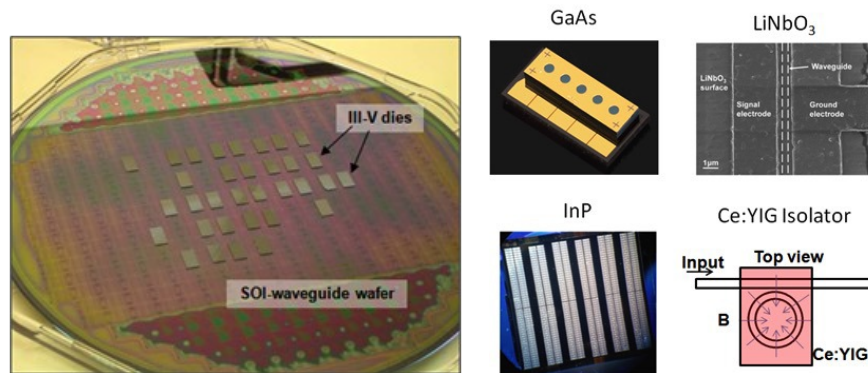


Figure 1. (left) Heterogeneous integration of III-V on 200 mm SOI wafer by multiple die bonding [26] (right) Heterogeneous integration with silicon has been demonstrated with various materials further extending capabilities of heterogeneous-silicon platform [28, 29].

The SOI platform by itself offers an almost complete suite of photonic components, including filters, (de)multiplexers, splitters, modulators, and photodetectors. However, electrically pumped efficient sources on silicon remain a challenge due to this material's indirect bandgap. A way to introduce efficient electrically pumped sources is to utilize III-V gain regions placed directly on silicon. There are three approaches to achieve this [1]. One approach [2] uses III-V chips bonded on silicon with coarse alignment and subsequently processed on the Si wafer scale (see Figure 1). This has the advantage of minimizing the area requirement of III-V material, thus minimizing the III-V epitaxial wafer cost. It has also the great advantage that very different epitaxial stacks (and not necessarily III-V materials alone) can be integrated together and processed simultaneously [5]. A second approach is the direct epitaxial growth of III-V layers on silicon or SOI using intermediate buffer layers, typically Ge and strained superlattices, to minimize dislocations propagating into the active region [6, 7]. The use of quantum dot (QD) laser gain material can minimize the effect of threading dislocations on threshold and output power, as efficient capture and localization of injected carriers by individual quantum dots greatly reduces non-radiative recombination at dislocations. Recent results show tremendous improvement in laser lifetime of epitaxially grown quantum dot lasers on silicon over similar quantum well lasers [8]. Although the improvement is significant, the lifetime is not yet adequate for most applications, but further progress is expected. A third approach is to combine these approaches: one can grow InAs QD gain material on silicon and then bond to patterned SOI wafers for efficient waveguide coupling and PIC fabrication. This could be on a wafer scale, directly up to 300 or 450 mm diameter wafers. It solves the wafer size limit for wafer scale III-V to silicon bonding, which has been restricted to 150 mm diameter, the maximum size of InP wafers available to date. Further, growth wafer reclamation when using smart cut or highly selective etching to perform substrate removal should be possible for cost reduction [1].

For it to be widely used, the heterogeneous-silicon PIC platform has to offer low power, low cost, high capacity, high volume, high yield and high reliability. Silicon wafer scale processing can offer high capacity, high volume and low cost. Publicly available studies suggest that the heterogeneous silicon platform is suitable for making reliable active optical devices, including lasers, modulators and photodetectors [9] and low power devices have readily been demonstrated [10, 11, 12, 13, 14] addressing all of the above requirements.

Heterogeneous integration on silicon can accommodate not only III-V materials that provide gain, detection and modulation, but can also include more exotic materials (Figure 1) such as LiNbO<sub>3</sub> and Ce:YIG bringing the promise of high performance modulators, nonlinearities (second-harmonic generation, parametric amplification, and entangled photon generation) and magnetic properties. LiNbO<sub>3</sub> based modulators on heterogeneous silicon platform are demonstrated either by thin-film direct wafer bonding [21] or by thin film bonding via benzocyclobutene (BCB) [22]. Performance, at this stage, is still limited at the few GHz range due to non-optimized designs with high RC constants and acousto-optic resonances, but substantial improvements are expected with more refined designs. Magneto-optical materials can be combined with silicon photonics to obtain optical non-reciprocity. Surface activated direct bonding [23] and direct deposition of magneto-optic material [24] have been demonstrated. The performance of the MZI silicon

waveguide optical isolator was demonstrated with an isolation of 30 dB at a wavelength of 1548 nm. In addition, a maximum isolation of 15.3 dB was obtained in an optical circulator fabricated with a silicon MZI waveguide [25].

Light generation on silicon chips can also be achieved by integration of rare-earth-ion (RE) doped dielectric thin films. The advantages of RE approach would be direct deposition onto silicon substrates, amplification of higher bit-rate signals without patterning effects, higher temperature of operation and inherent narrow linewidth. Disadvantages are significantly lower gain in range of few dB/cm and a need for optical pumping [89].

Some intrinsic limitations of all-silicon devices can also be overcome by combining conventional SOI waveguides with organic cladding material in a concept of silicon-organic hybrid integration. This approach has demonstrated extremely efficient modulators consuming only 0.7 fJ/bit to generate 12.5 Gbps data stream [90].

### 3. OPTICAL INTERCONNECTS

Although operating frequency and sequential processor performance has slowed down, the scaling of Moore's Law continues by increasing the number of processor cores while keeping total power consumption constrained due to total power budget roughly assumed to be around 200 W [88]. This is achieved by increasing the number of cores and transistors on die (modern processors are approaching 10 billion transistors on a single chip), making them more power efficient and utilizing more advanced power conservation technologies. The scaling of number of cores is expected to have a limit due to Amdahl's Law that limits the performance gain per core as number of cores is increased, but currently we are still in the exponential growth phase. As the number of cores is increasing, the capacity of interconnects between individual cores and between the processor and outside world also has to increase. Currently this communication is done by electrical interconnects and once the wiring fills all the available space, it has been shown that the capacity cannot be increased by changing the system size [15]. The limit to the total number of bits per second of information that can flow in a simple digital electrical interconnection is set only by the ratio of the length of the interconnection to the total cross-sectional dimension of the interconnect wiring - the "aspect ratio" of the interconnection. This limit is largely independent of the details of the design of the electrical lines, and because it is scale-invariant, it cannot be changed by either growing or shrinking the system. Performance can be improved by using repeaters, advanced coding and multilevel modulations, but these techniques also have limitations, one of which is the energy efficiency as total power has to be kept to around 200 W of thermal budget. Optical interconnects have a potential to solve this problem since they avoid the resistive loss physics that give this limit.

The three key metrics for future interconnect technology are bandwidth density, energy efficiency and latency [16]. Optical links have all but replaced electrical links for telecommunications applications and are replacing data-communications interconnect links at increasingly short lengths. Currently it is not clear when optics will also be the enabler for on-chip communications and enable an optical network-on-chip (NoC) for communication between multiple cores. This will only happen when optical interconnects can clearly outperform electrical interconnects on the combination of these three key metrics. Projections are that this typically means a  $\sim 100$  fJ/bit system energy target, with about 10–20 fJ/bit allocated for the optical source [17]. Record 100G high-speed transceivers are currently at 10 pJ/bit [10]. For slower 5 Gbit/s intra-chip silicon electronic-photonic links values as low as 250 fJ/bit are quoted [11], but they do not take the wall-plug efficiency of the laser into account. For just sources, values as low as 14 fJ/bit were demonstrated at bit rates of 12.5 Gbit/s [12]. Current studies show that optical interconnects are not yet a feasible option for on-chip communication due to lack of improvements in terms of bandwidth and energy consumption [18], but as CMOS nodes continue scaling down, optical interconnects will become more and more interesting. One of the reasons is that at small enough nodes, the transistor capacitances become small enough to be directly driven by a photodetector. This can eliminate the trans-impedance amplifier and greatly reduce the power consumption of the receiving portion of the link [19].

At this point it is unclear when optical interconnects will become a design of choice for on-chip communications, but it is clear that at the present rate of progress, electrical interconnects will not be able to keep up within the next decade. Optics, as it is not limited by resistive loss, is currently the strongest candidate for future on-chip communications. As the length of interconnects grows to cm range, it is expected that optics will replace copper even sooner. The baud rate of a single channel will not likely scale much with the move to optics as the accompanying fast electronics increases power consumption and is likely to be around 25 Gbps over the next decade [17]. As optics is also limited by the size of waveguides, there is a limit in the number of optical channels that can be packed around the edge of chip. To satisfy the bandwidth requirements, future systems will generally be wavelength-division multiplexed (WDM) ones. In order to

generate a large number of wavelengths from a single source, comb lasers are considered [17]. A challenge with densely packed WDM channels is thermal control of individual components. Active control uses energy and may not be suitable for integration with devices generating around 200 W of heat in a small volume, while passive temperature control brings its own set of tradeoffs. We briefly overview thermal tuning and athermal operation in Section 4.2. To further increase available bandwidth, vertical stacking of waveguides on chip could be employed.

Close integration of electronics with photonic integrated circuits (so called “Smart Photonics”) also benefits photonics as it allows low-power, high-impedance drivers avoiding low-efficiency 50  $\Omega$  terminations [10], and allows for smart photonic circuits with self-calibration and active-feedback control on-chip in real time with reduced power consumption [20].

To conclude the interconnect section, it is clear that electrical interconnects will not be able to keep up with bandwidth demand in the long term. Optical interconnects provide an alternative that could overcome this limitation once performance on all three key metrics is sufficiently better than what is available in copper. The trend is evident as optical interconnects continuously push copper links to shorter and shorter lengths due to their inherent limitations. Furthermore, the close integration of driving electronics with photonic integrated circuits allows added flexibility and reduced power consumption.

#### 4. SILICON PHOTONICS PASSIVES

The range of passive optical components demonstrated on silicon is extremely impressive and includes waveguides, couplers, multiplexers, polarization control devices, filters, resonators, etc. [29, 32]. Silicon ( $n_{Si} = 3.48$ ) and its oxide ( $n_{SiO_2} = 1.48$ ) form high-index contrast, high-confinement waveguides ideally suited for medium to high-integration and small passive devices in their transparency wavelength range, including the most important 1300 and 1550 nm communication bands (Figure 2). Tight bends with losses lower than 0.09 dB for bending radii of only 1  $\mu\text{m}$  have been demonstrated more than ten years ago [33], and propagation losses below 1 dB/cm have been shown in both communication bands allowing for compact and excellent performing passive devices.

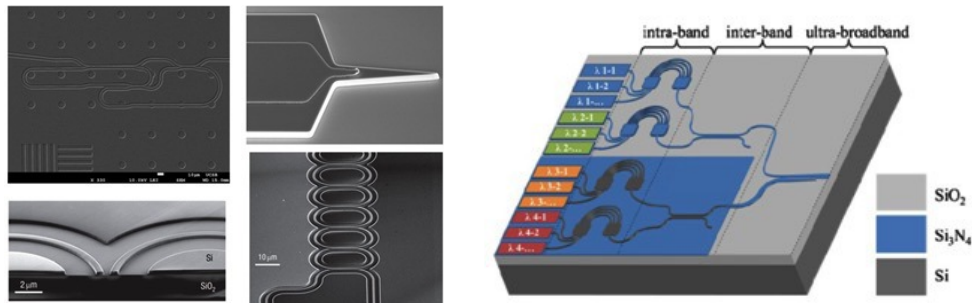


Figure 2. (left) Si/SiO<sub>2</sub> material system offers superior waveguide capabilities due to high index contrast and maturity of Si processing allowing for very small wires and tight bends [30, 31] (right) Schematic design of multi-octave spectral beam combiner with integrated lasers utilizing Si and Si<sub>3</sub>N<sub>4</sub> waveguides [39].

Record low losses in silicon, less than 3 dB/m at 1600 nm, have been reported in [34], calculated by the internal Q factor of silicon ring resonators of  $2.2 \times 10^7$ . The authors further conclude that the measured loss is still limited by bend loss in this low-confinement configuration with very low sidewall interaction, so the pure propagation loss could be even lower. Such record values are probably not suitable for wide integration as the radius of said ring was 2.45 mm. By increasing the confinement, the bend loss goes down at the expense of higher propagation loss, mainly due to scattering at vertical sidewalls. Nevertheless, complex devices with much smaller bend radii and measured propagation loss <0.5 dB/cm in C-band [35] and <0.7 dB/cm in O-band [36] have been demonstrated.

For even lower losses, one can turn to the Si<sub>3</sub>N<sub>4</sub> waveguide platform that offers more than two orders of magnitude lower propagation loss (as low as 0.045 dB/m) [37]. The Si<sub>3</sub>N<sub>4</sub> waveguides can readily be integrated with the silicon platform with coupling losses between 0.4-0.8 dB per transition depending on taper bandwidth [38]. Another benefit in using Si<sub>3</sub>N<sub>4</sub> waveguides is the absence of two-photon absorption and the resulting free-carrier absorption present in Si waveguides, but the downside is lower confinement and larger minimum bend radii.

The heterogeneous silicon platform has been shown to be usable with an extremely broad wavelength range. The platform is capable of combining optical frequency bands spanning 4.2 octaves from ultraviolet to mid-wave infrared into a single, low  $M^2$  output waveguide as demonstrated in (Figure 2) [39]. Using two waveguide types (silicon nitride and silicon), the prohibitively high material losses that would be present in a single waveguide platform for UV to mid-IR wavelengths are avoided while providing a platform compatible with heterogeneous integration of laser sources covering the same spectral range. This concept shows that an integrated array of lasers spanning UV to mid-IR bands spectrally combined into a single output waveguide for high power and ultra-broadband applications is feasible.

#### 4.1 On-chip polarization handling devices

A polarization beam splitter (PBS) is a key component for separating or combining two orthogonal polarization modes (i.e., TE and TM polarizations), which is very important for photonic integrated circuits, e.g. modern 100G transceivers utilize dual-polarizations for reducing the baud-rate. One can also envision polarization discrimination based sensors whose front-end is fully integrated on chip. PBSs have been reported using various structures including multimode interference structures, directional couplers (DC), Mach-Zehnder interferometers, and photonic-crystal (PhC)/grating structures [32]. Most of the realizations are quite long physically, making integration more difficult, or require introduction of large stress or the use of highly birefringent materials such as LiNbO<sub>3</sub>, III-V semiconductor compounds or liquid crystal. Another approach is using PhC or out-of-plane gratings. An overview of PBS structures with typical lengths is given in [40]. The same paper also proposes an asymmetrical directional coupler that utilizes evanescent coupling between a strip-nanowire and a nanoslot waveguide. Although such a design allows for a very short structures (less than 10  $\mu\text{m}$ ), the difficulty is the fabrication of the nano-slot. A structure with relaxed fabrication tolerance based on an asymmetrical bent DC using silicon-on-insulator nanowires is introduced theoretically [41] and demonstrated experimentally [42]. The bent DC is designed to cross-couple TM polarized light completely while there is almost no coupling for TE polarization. This is done by designing the bent coupling section to be phase-matched only for TM polarization. Once polarizations are separated into two waveguides, one of the polarizations can be rotated so both waveguide arms have identical polarizations.

Realization of on-chip polarization rotation is challenging as planar waveguides usually maintain polarization. A polarization rotator using an SOI nanowire with a cut corner has been demonstrated [43]. The cut corner almost fully hybridizes two lowest-order modes, so light entering the polarization rotator excites these two hybridized modes and two-mode interference takes place. Polarization rotation is made possible in only  $\sim 7 \mu\text{m}$  of length. A modified polarization rotator configuration fabricated using a four etch-step CMOS-compatible process including layer depositions on a silicon-on-insulator wafer has been demonstrated experimentally [44].

These two functions can be integrated in a single structure as proposed in [45]. Here an ultra-compact polarization splitter-rotator is proposed by utilizing a structure combining an adiabatic taper and an asymmetrical directional coupler. The input TE polarization does not change when it goes through the adiabatic taper structure and is not coupled to the adjacent narrow waveguide due to phase mismatch. Fundamental TM polarization launched at the same port is first efficiently converted to higher-order TE mode in the adiabatic taper structure and is then coupled to TE fundamental mode of the adjacent narrow waveguide. The total device length is less than 100  $\mu\text{m}$  and the design utilizes only one etch step.

#### 4.2 Tuning and thermal stability

Devices based on silicon are readily thermally tunable owing to the large thermo-optic coefficient ( $dn/dT$ ) of silicon. A value of  $dn/dT$  of  $1.87 \times 10^{-4} / \text{K}$  at room temperature and 1.5  $\mu\text{m}$  is generally reported and the coefficient increases at shorter wavelength to  $1.94 \times 10^{-4} / \text{K}$  at 1.3  $\mu\text{m}$  [46]. The highly-efficient temperature tuning has been used to realize tunable filters, switches, add/drop multiplexers, and widely-tunable lasers among others. Due to being thermal in nature, tuning is relatively slow in the  $\mu\text{s}$  to ms range, as summarized for switches [47]. There is usually a trade-off in terms of tuning efficiency and speed, and the trade-off is related to thermal isolation of the tuning section. In the case of low thermal resistance, the heaters are less efficient in terms of power, but are faster as heat can dissipate more quickly. In terms of efficiency, switches have been demonstrated with switching powers of only 0.6 mW at the expense of switching speed that is 3.6 ms [13]. Tuning ranges of 20 nm for a single ring structure have been demonstrated [48] and wider tuning range is easily obtained by utilizing a Vernier effect. We return to wide-tunability in Section 6.2.

The high thermo-optic coefficient can also be a disadvantage if one wants to realize athermal devices that do not require power hungry and inefficient thermoelectric cooling units. Various athermal designs have been studied [49, 50, 51]. The simplest athermal technology is the athermal waveguide. By co-integrating waveguides with different thermo-optic

coefficients, and adjusting the length of each waveguide type, the phase difference between the neighboring waveguides can in principle be independent of temperature, over a range in excess of 50 K. Such an approach has extensively been used in e.g. athermal arrayed-waveguide-gratings [52]. Unfortunately, the same approach is less well suited for devices whose response depends on the absolute phase shift such as ring resonators or Bragg gratings. One method of thermal stabilization of such structures is to adopt an upper cladding made of a material with negative thermo-optic coefficient to compensate for the positive thermo-optic coefficient of silicon. By using polymer claddings with  $dn/dT$  of  $-2.65 \times 10^{-4}/K$ , ring prototypes with temperature dependent resonant wavelength shift of only 0.5 pm/K were demonstrated [53]. Titanium dioxide also has a strong negative thermo-optic coefficient of  $\sim -(1-2) \times 10^{-4}/K$ , and is compatible with CMOS processes offering superior reliability than polymers. Thermal sensitivities of only  $-2.9$  pm/K were demonstrated [51]. Athermal laser designs are described in [49] and uncooled athermal WDM lasers with channel spacing of 200 GHz have been demonstrated operating from 20 °C to 80 °C without significant change of wavelength [5].

## 5. HETEROGENEOUS SILICON PHOTONICS ACTIVE DEVICES

Since the first report of the electrically pumped heterogeneous silicon laser [54], a full suite of heterogeneous silicon III-V components has been developed [29]. Here we shall briefly mention some of recent record performing heterogeneous-silicon devices.

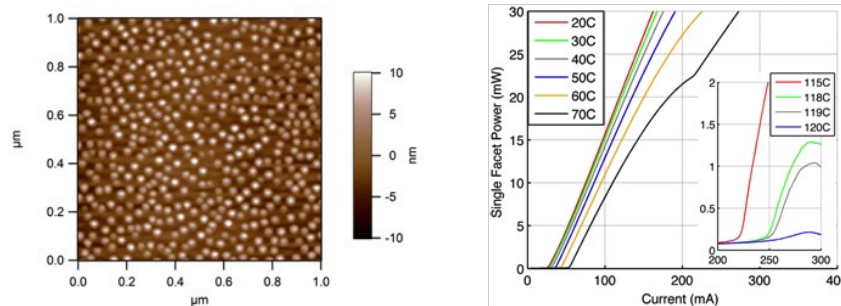


Figure 3. (left) A  $1 \times 1 \mu\text{m}^2$  AFM scan of the InAs quantum dots grown on Ge-on-Si substrates. [66] (right) A 1mm x  $5 \mu\text{m}$  ridge waveguide Fabry-Perot quantum dot laser on Ge/Si demonstrating continuous wave lasing up to 119°C [6].

Ridge waveguide lasers at 1.3  $\mu\text{m}$  fabricated from InAs QDs grown on silicon by molecular beam epitaxy (Figure 3) have shown room temperature continuous wave thresholds as low as 16 mA, output powers exceeding 176 mW, and lasing up to 119 °C [6]. The reliability of epitaxially grown InAs/GaAs lasers on silicon has improved tremendously and is now quoted at 4600 hours [8], bringing the promise of wafer scale growth on silicon and allowing direct bonding with wafer sizes of up to 450 mm once reliability is further improved.

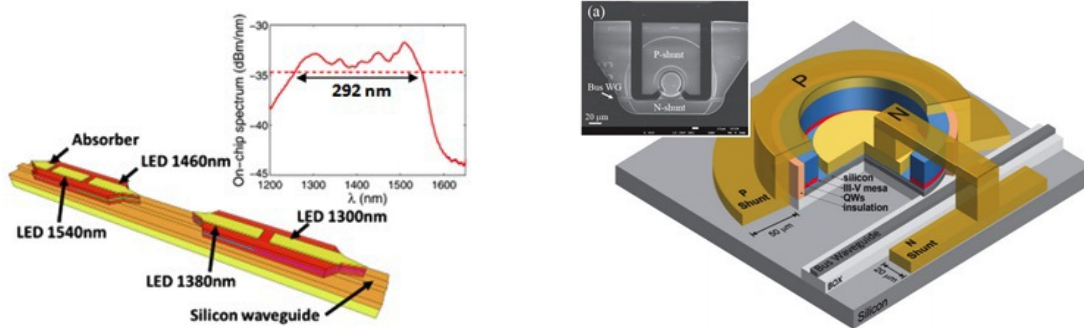


Figure 4. (left) Illustration of the broadband LED and (inset) balanced pumping to optimize the 3 dB bandwidth. The pumping currents were 70, 50, 300, and 140 mA for the sections at 1300, 1380, 1460, and 1540 nm [55]. (right) The diagram of a heterogeneous silicon microring (HSMR) laser with double thermal shunt design. (right inset) plain-view SEM images of a HSMR laser with double thermal shunt design. Metal shunts were realized with gold [58].

A broadband superluminescent III-V-on-silicon light-emitting diode (LED) with 292 nm of 3 dB bandwidth and on-chip power of -8 dBm was demonstrated [55]. To achieve the large bandwidth, quantum well intermixing and multiple die bonding of InP on a silicon photonic waveguide circuit were combined. The device consists of four sections with

different bandgaps, centered around 1300, 1380, 1460, and 1540 nm (Figure 4). The fabricated LEDs were connected on-chip in a serial way, where the light generated in the smaller bandgap sections travels through the larger bandgap sections.

Colliding-pulse mode-locked laser diodes on heterogeneous silicon platform were investigated and characterized [56]. Reduction in microwave linewidth using two techniques has been demonstrated. First, reducing the number of quantum wells reduces the confinement factor, thereby lowering the spontaneous emission contribution to the linewidth. Second, a  $\sim 4$  cm long on-chip passive feedback cavity is used to provide optical feedback to stabilize the laser and further reduce the linewidth. The linewidth achieved for passive mode locking at 17.36 GHz using the above two techniques is 29 kHz.

Low threshold (8.8 mA) and high speed (9.5 GHz) short cavity distributed feedback (DFB) heterogeneous silicon lasers were demonstrated [57]. The large direct modulation bandwidth of the heterogeneous short cavity DFB shows its potential as a low cost and low power laser source.

There has also been progress on low threshold heterogeneous silicon microring lasers [14]. The improvement in performance comes by selective reduction of the active region volume. This is done by appropriately undercutting the multiple quantum well (MQW) active region to force carriers to flow toward the outer edge of the microring for better gain/optical mode overlap. A reduction of the threshold to 3.9 mA and up to 80% output power enhancement is observed, mainly due to the improved injection efficiency. Thermal management of heterogeneous silicon ring lasers was also explored [58]. By improving the thermal impedance of microring lasers with a novel double gold thermal shunt design (Figure 4), continuous-wave lasing up to 105 °C was demonstrated. This high temperature operation is important for these lasers are to be used in interconnect applications in un-cooled environments, such as data centers. Further improvement is possible, by using metals with higher thermal conductivity, such as copper, which is also CMOS process compatible, to optimize the efficiency of the thermal shunts.

The silicon photonics transmitter chip was successfully integrated with a low power CMOS driver chip with a flip-chip bonding method [59]. The transmitter chip with 16 channel electro-absorption modulator (EAM) array was aligned and bonded with high speed VLSI circuits with high yield. The heterogeneous EAM with 100  $\mu$ m length had an extinction ratio larger than 6 dB for 1 V voltage swing with the optical bandwidth over 20 nm in C band. The integrated EAM had an open eye at 12.5 Gbps with 3.5 dB extinction ratio at 1510 nm, with the maximum driving voltage swing from zero to 2.4 V.

Extremely low thresholds of 31  $\mu$ A were shown for continuous-wave operation of lambda-scale embedded active-region photonic-crystal lasers (LEAP) at room temperature fabricated on a Si wafer [12]. As LEAP has emission in a direction normal to the wafer, the light was coupled via grating couplers. The maximum output power is 0.27  $\mu$ W at an injected current of 200  $\mu$ A, which includes around 10 dB of optical coupling loss of the measurement setup. The maximum output power from the device is estimated at few  $\mu$ W.

The heterogeneous silicon platform has also been extended to non-communication wavelengths such as 2  $\mu$ m [64]. Room temperature, continuous wave 2.0  $\mu$ m wavelength lasers were heterogeneously integrated on silicon by molecular wafer bonding of InGaAs quantum wells grown on InP. These heterogeneous silicon lasers operate continuous-wave up to 35°C, have threshold currents as low as 59 mA and emit up to 4.2 mW of single-facet CW power at room temperature. These lasers should enable the realization of a number of sensing and detection applications in compact silicon photonic systems.

Heterogeneously integrated waveguide-coupled photodiodes on SOI with 12 dBm output power at 40 GHz have been demonstrated [61]. The InP-based modified uni-traveling carrier photodiodes on SOI waveguides have internal responsivity of up to 0.95 A/W and have the highest reported output power levels at multi-GHz frequencies for any waveguide photodiode technology including native InP, Ge/Si, and heterogeneously integrated photodiodes. The reasons for the exceptional performance lie in the added flexibility introduced by heterogeneous process that allows independent change of the widths of the Si waveguide and III-V mesa. This allowed simultaneous reduction of current crowding and a tailored absorption profile to reduce saturation effects via mode and bandgap engineering.

## 5.1 Sensors on chip

The ability to integrate multiple material systems on the heterogeneous silicon platform presents the possibility of designing fully-integrated sensors on chip. Recently there have been proposals for integrated waveguide optical gyroscopes [62] and magnetometers [63]. A highly integrated optical gyroscope using low loss silicon nitride waveguides and integration of all the required active and passive optical elements on a chip is possible with a detection

limit on the order of  $19^\circ/\text{hr}/\sqrt{\text{Hz}}$ . This is for an area smaller than  $6.5 \text{ cm}^2$  with a propagation loss of  $1 \text{ dB/m}$  in a ten meter long waveguide [62]. The analysis of novel highly sensitive optical magnetometers using low-loss silicon nitride waveguides shows that with recent advances in Ce:YIG pulsed laser deposition on silicon nitride, sensitivities on the order of  $20 \text{ fT}/\sqrt{\text{Hz}}$  at room temperature in an area  $<1 \text{ cm}^2$  should be possible. All the required elements can be fully integrated on a chip using the heterogeneous silicon platform. By using materials with greater sensitivity to magnetic field, like  $\text{Bi}_x\text{Ce}_{3-x}\text{Fe}_3\text{O}_{12}$ , the minimum achievable sensitivity could be further improved by a factor of two [63].

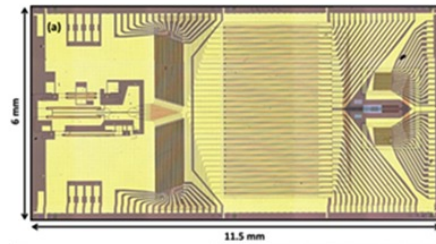


Figure 5. Confocal microscope picture of the fully integrated beam-steering PIC. [65].

The most complex heterogeneous PIC is a fully-integrated free-space beam-steering photonic integrated circuit (Figure 5) consisting of 164 optical components including lasers, amplifiers, photodiodes, phase tuners, grating couplers, splitters, and a photonic crystal lens. The PIC exhibited steering over  $23^\circ \times 3.6^\circ$  with beam widths of  $1^\circ \times 0.6^\circ$  giving a total of 138 resolvable spots in the far field with 5.5 dB background suppression [65].

## 6. NARROW-LINEWIDTH LASERS

Narrow-linewidth is becoming increasingly important in modern communications and sensors. Modern 100G transceivers utilize dual-polarization quadrature-phase-shift-keying (DP-QPSK) in order to send 4 bits simultaneously (2 in each polarization) and reduce the symbol speeds to 28 Gbaud. Moving to higher transmission-speeds at a single wavelength such as 200G and 400G while keeping the same symbol speeds necessitates using even more advanced modulation formats, such as DP-16QAM or DP-256QAM where QAM stands for quadrature amplitude modulation. Such advanced modulations require lasers and local oscillators for demodulation with very low phase noise, or narrow-linewidth. For square 16-QAM constellation, the linewidth should be  $<100 \text{ kHz}$  and for square 64-QAM linewidth should be  $<1 \text{ kHz}$  assuming 28 Gbaud rate [67]. Traditional III-V lasers had linewidths in MHz range and only recently have been able to demonstrate sub-MHz and finally sub-100 kHz linewidth with careful optimization of the resonator and the gain sections [68-74]. It should be noted that a direct comparison between quoted values is sometimes hard to make as methods to measure and quote linewidths differ. Heterogeneous-silicon lasers have been showing sub-MHz linewidths for some time and recently have shown results significantly surpassing the performance of pure III-V lasers [31, 35, 36, 75-82]. A comparison is shown in Figure 6. In both, single-wavelength and widely-tunable lasers, a key enabler for narrow linewidth with heterogeneous designs lies in utilization of low-loss silicon waveguides and high-Q resonators.

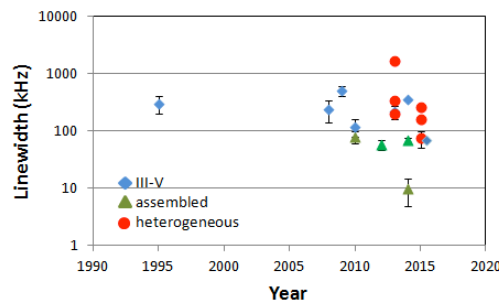


Figure 6. Widely-tunable integrated lasers linewidth vs. year. We make distinction between III-V lasers, and assembled (butt-coupled chips) or heterogeneous (single-chip, monolithic) silicon laser designs [31, 35, 36, 68-82].

## 6.1 Single-wavelength lasers

The linewidth of single-frequency semiconductor lasers is inherently broader than e.g. that of solid-state lasers. In a semiconductor laser there are two mechanisms broadening the linewidth: (1) the spontaneous emission which alters the phase and intensity of lasing field and (2) the linewidth enhancement factor  $\alpha$  that characterizes the coupling between intensity and phase noise and is specific to semiconductor lasers due to carrier density fluctuations. There has been continuous effort to improve the linewidth or coherence, and for DFB lasers methods included: long cavities, longitudinal mode engineering via multiple phaseshifts, optimization of the active medium (e.g. introducing strain), and wavelength detuning.

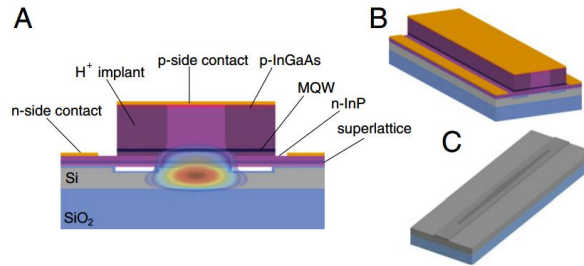


Figure 7. High- $Q$  heterogeneous laser device schematics (not to scale). (A) Two-dimensional cross-section of the heterogeneous platform, with superimposed optical transverse mode profile. (B) Perspective view of a high- $Q$  heterogeneous laser. (C) Perspective view of the high- $Q$  silicon resonator [83].

The heterogeneous silicon photonics platform opens up a new possibility in improving the coherence by providing a mechanism to separate the photon resonator and highly-absorbing active medium [83] as shown in Figure 7. The quality factor of conventional III-V semiconductor lasers is limited by free carrier absorption in the heavily doped p- and n-type cladding regions, as well as in the active region where photons, both spontaneous and induced, are generated. There is an inevitable compromise resulting from carrying out both photon generation and photon storage in the same III-V material. By creating high- $Q$  photon storage in silicon and using III-V for gain, the best of both worlds can be combined.

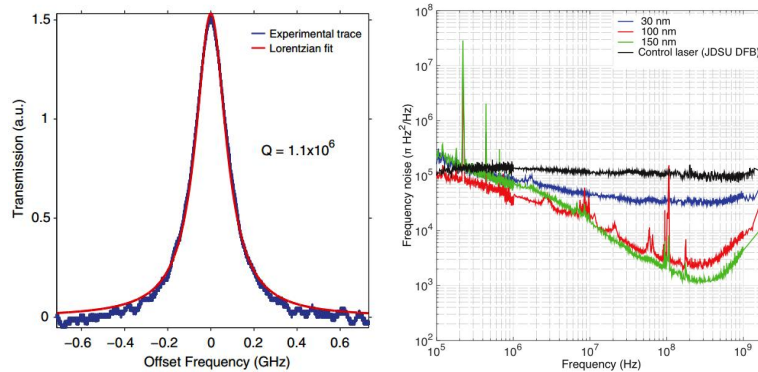


Figure 8. (left) Experimental trace and Lorentzian fit of the transmission resonance of a high- $Q$  silicon resonator. The  $Q$  is estimated at 1.1 million [84]. (right) Frequency noise spectral density for three high- $Q$  heterogeneous lasers (with different spacer thickness) and control laser. The spacer is layer of low refractive index material ( $\text{SiO}_2$ ) between the silicon waveguide and III-V material. A noise floor, set by phase noise injected by the EDFA used to amplify the laser signal, limits the measurement of the thickest spacer heterogeneous. This is evident in the noise rise at higher frequencies and was found to vary with the amount of amplification. At the lowest point ( $\sim 1$  kHz), the laser and amplifier contribute approximately equal noise, hence putting the intrinsic laser linewidth well below the 1 kHz mark [85].

The total  $Q$  of a heterogeneous resonator can then be expressed as:

$$\frac{1}{Q} = \frac{\Gamma}{Q_{III-V}} + \frac{1-\Gamma}{Q_{Si}} \quad (1)$$

where  $\Gamma$  is the mode confinement factor in III-V. By tailoring the transverse geometry, the modal confinement can be engineered and total  $Q$  can be optimized for best performance. Removing light from III-V appears counterintuitive because it reduces the modal gain available to the laser; however, in the limit that the  $Q_{\text{III-V}}$  term dominates the total  $Q$ , the reduction in modal gain is exactly balanced by a reduction in total modal loss, and thus the threshold carrier density remains constant. Increasing the quality factor of the laser cavity and keeping the same modal confinement provides a double benefit to phase noise by reducing the number of excited carriers needed to reach threshold, thus decreasing spontaneous photon generation while increasing photon storage. By designing a high- $Q$  silicon resonator with  $Q = 1.1 \times 10^6$  (Figure 8) and having a  $\Gamma = 15\%$ , linewidths as low as 18 kHz were demonstrated. This is approximately 200x improvement compared to previously reported results. The linewidth is measured by the FM discriminator method, and quoted number corresponds to the high-frequency white-noise floor limit. Specifics of the silicon resonator design are given in [84].

With further optimization and introduction of a spacer layer, the mode confinement factor was reduced to as low as 1.5% in III-V and to only 0.2% in QW region (Figure 9). Spacer is layer of low refractive index material ( $\text{SiO}_2$ ) between the III-V and silicon, and was used to directly control the rate of spontaneous emission into the lasing mode. This further increased the  $Q$  factor of the laser mode and reduced the linewidth below 1 kHz, as measured by the FM discriminator method quoting the white-noise limit [85]. This result shows that, not only the heterogeneous silicon platform can perform as good as a native III-V one, but can in fact offer more than order-of-magnitude better performance.

## 6.2 Widely-tunable lasers

Passive microring-resonator-coupled semiconductor lasers were proposed in 2001 [86]. In such a structure, an active region in the conventional Fabry–Perot cavity is coupled with a passive ring resonator. This is different from conventional ring lasers, where the active traveling wave ring resonator replaces the standing wave Fabry–Perot cavity. The ring inside the cavity improves side mode suppression ratio, linewidth, and decreases the frequency chirp. The concept can be extended to two or more rings, significantly improving the single-mode tuning range by utilizing the Vernier effect [87].

Using rings inside the cavity benefits the linewidth in two ways: (1) increasing the photon lifetime due to effective cavity length enhancement, and (2) providing negative optical feedback by slight detuning from the ring (resonator) resonance. Both mechanisms cannot be maximized at the same time, but there is an optimal point where the combined influence is maximized. The combination of ring resonators and cavity mirror (facet mirror, loop mirror, etc.) can be thought of as a frequency-dependent passive mirror with complex amplitude reflectivity  $r_{\text{eff}}(\omega)$ . The linewidth improvement [60] due to feedback from this frequency dependant mirror is given by factor  $F^2$  where  $\Delta\nu$  and  $\Delta\nu_0$  are the linewidths with and without the  $r_{\text{eff}}(\omega)$  mirror (Figure 9).

$$\Delta\nu = \frac{\Delta\nu_0}{F^2} \quad (2)$$

$$F = 1 + A + B \quad (3)$$

$$A = \frac{1}{\tau_{\text{in}}} \text{Re} \left\{ i \frac{d}{d\omega} \ln r_{\text{eff}}(\omega) \right\} \quad (4)$$

$$B = \frac{\alpha_H}{\tau_{\text{in}}} \text{Im} \left\{ i \frac{d}{d\omega} \ln r_{\text{eff}}(\omega) \right\} \quad (5)$$

where  $\alpha_H$  is the linewidth enhancement factor.  $\tau_{\text{in}} = 2n_{\text{eff}}L_a/c$  where  $n_{\text{eff}}$  is the effective index of the gain section,  $L_a$  is the length of active region and  $c$  is the speed of light. The  $A$  term, corresponding to the linewidth reduction from reduced longitudinal mode confinement, is often denoted as the ratio of the external (passive section) cavity path length to the gain section path length. As the effective length of a ring resonator is maximized at resonance, the  $A$  factor is maximized when the ring is placed exactly at resonance. The effective length of the ring ( $L_{\text{eff}} = -d\phi/d\beta$ ) can be approximated at resonance and with losses ignored by:

$$L_{\text{eff}} = \frac{1 - \kappa^2}{\kappa^2} L_{\text{ring}} \quad (6)$$

For a weakly coupled rings ( $\kappa \ll 1$ ), the effective length will be largely extended and can even dominate the total cavity length. The  $B$  term corresponds to the reduction from the negative feedback effect where a decrease in wavelength increases reflectivity (increasing photon density in the cavity) and hence decreases carrier density, which in turn causes the wavelength to increase due to the carrier plasma effect. The phase condition in the cavity can be used for a slight detuning of the laser oscillation with respect to the minimum cavity loss condition (resonator resonance). This negative feedback effect occurs only on the long wavelength side of the resonance and is optimum at the wavelength of highest slope in the transmission spectrum. At the ring resonance, i.e. the optimal condition for the  $A$  term, it is equal to zero. On the short wavelength side of the resonance, the effect is reversed and operates in positive feedback, broadening the linewidth. The combined effect of  $A$  and  $B$  is at maximum when the laser is slightly detuned on the long wavelength side (lower frequency), as shown in Figure 9.

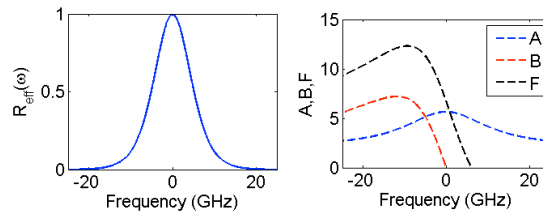


Figure 9. (left) Normalized reflection of ring-resonator and cavity mirror combination (right) Linewidth reduction factor of the laser as a function of frequency offset from resonance calculated using eqs. 2,3,4 and 5 ( $\alpha_H=4$ ). The combined effect of both contributions is maximized at slight offset to lower frequencies than the ring resonance. [36].

We believe that these two mechanisms - the effective cavity length enhancement and the negative optical feedback - are responsible for the exceptional linewidth results shown by ring-coupled lasers. As the loss in rings ultimately limits the performance (obtainable  $Q$ ), the low-loss silicon waveguide platform is the key enabler of the exceptional performance shown by recent devices. We now turn to some specific widely-tunable narrow-linewidth lasers realized by ring resonators. We make a distinction between heterogeneous (single-chip, monolithically-integrated) and hybrid (assembled using butt-coupling between Si and III-V regions, multiple-chips) designs.

Heterogeneously-integrated ring-based Vernier lasers [78] featured a linewidth of 330 kHz. An improved design, coupled-ring-resonator (CRR) lasers [31, 79] have shown linewidth of 160 kHz (Figure 10). In both cases the linewidth was measured by delayed self-heterodyne technique. The advantage of using a CRR mirror design is a higher external differential quantum efficiency by avoiding having a drop port bus waveguide to form the necessary filter shape and having a simple two output-port laser. The threshold currents are around 50 mA with output powers in  $>15$  mW range.

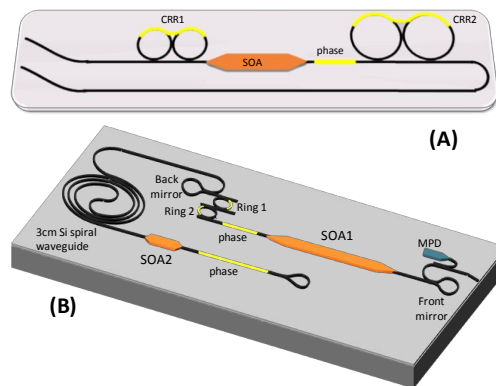


Figure 10. (A) Coupled-ring-resonator (CRR) laser. CRR acts as a mirror [31, 79], (B) Monolithically-integrated external-cavity lasers utilize a  $\sim 4$  cm long external cavity to reduce the linewidth [36].

Further progress has been made with a monolithically integrated external cavity [36]. A  $\sim 4$  cm long on-chip cavity is made possible by a low-loss silicon waveguide platform. Tuning in excess of 54 nm in the O-band as well as significant reduction in laser linewidth due to controlled feedback from the external cavity were shown. The linewidth measured with the delayed self-heterodyne method in full tuning range is below 100 kHz and the best results are around 50 kHz. The threshold current is in the 30 mA range, output power is  $>10$  mW and side-mode suppression ratio exceeds 45 dB across the entire tuning range.

The design of this laser is shown in Figure 10. The gain section (SOA1) is inside a 2 mm long cavity formed by loop-mirrors. The lasing wavelength is determined in the tuning section comprising two ring resonators and a cavity phase section, all of which are controlled by thermal phase tuners. The front loop mirror (at the output of the laser) has a 10% power reflection and the output of the laser is terminated at the facet at an angle of  $7^\circ$  to minimize reflections. The back loop mirror, after the wavelength tuning section, has a power reflection of 60%, which couples part of the light to the external cavity. In order to allow for a long external cavity, a low-loss waveguide platform is needed. Optimized silicon waveguides with a loss of 0.67 dB/cm at 1310 nm were used. The external cavity is  $\sim 4$  cm long and has its own phase adjustment section and gain section (SOA2). As the propagation loss in Si waveguides is very low ( $\sim 5$  dB loss per round-trip), there is quite strong feedback from the external cavity. The feedback is present even when SOA2 is reverse-biased, possibly from reflections at the tapers to the gain region or due to insufficient attenuation of the reverse-biased SOA2.

The SOA1 bias currents, for measured linewidths, were between 75 and 128 mA ( $\sim 2.5$ - $4.2 \times I_{th}$ ), while the external SOA2 bias currents were between 0 and 13.06 mA. The bias for external SOA2 is typically below transparency, potentially limiting the linewidth improvement performance due to increased noise in the feedback signal owing to random spontaneous emission events. Even lower linewidths (below 20 kHz) were measured at higher currents supplied to external SOA2, but the laser would become multimode with mode spacing determined by the external cavity length ( $\sim 1$  GHz) as the ring tuning section could not filter out a single longitudinal mode. In this case the RIN and frequency noise spectrums have peaks at this mode separation. This shows that the external cavity can provide even better performance if the filtering section is optimized and SOA is replaced by a variable optical attenuator to control the level of feedback. Further improvement is expected by packaging the devices. Nevertheless, to the best of our knowledge, these results set a world record linewidth for a heterogeneously-integrated widely-tunable laser design.

Extremely impressive results were achieved by an assembled hybrid-design using butt coupling between InP and Si chips shown in Figure 11 [35]. The authors have demonstrated wavelength tunable lasers by passive alignment techniques with over 100-mW fiber-coupled power (using a booster SOA) and linewidth narrower than 15 kHz along the whole C-band (Figure 11). Record linewidth values as low as 5 kHz are quoted. Linewidth is again measured by delayed self-heterodyne method. As main reasons for exceptional performance, very low loss Si-wire waveguides (with losses lower than 0.5 dB/cm in C-band) and hybrid-integration are quoted.

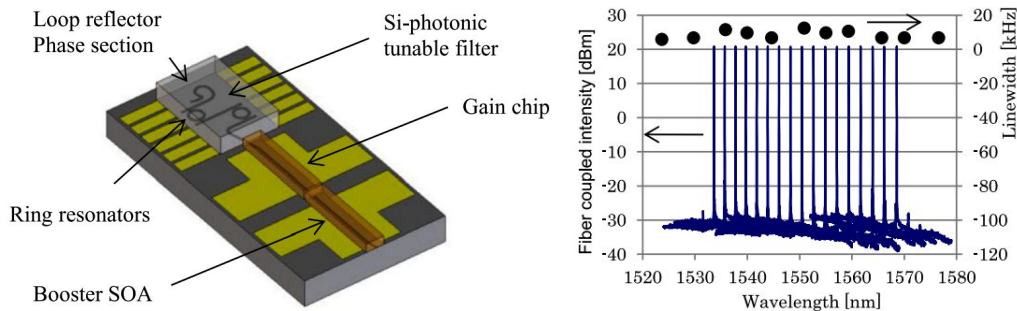


Figure 11. (left) A schematic view of an assembled butt-coupled widely-tunable narrow-linewidth laser. The laser consists of Vernier ring filter made in silicon and two III-V gain chips, one as a gain element inside the laser cavity and one as a booster SOA that can also be used as an OFF switch (right) Superimposed spectra and measured linewidth as a function of wavelength. Fiber coupled power is  $>20$  dBm and linewidth is  $<15$  kHz across full C-band [35].

### 6.3 Narrow-linewidth using High- $Q$ rings

We have theoretically analyzed the use of fully-integrated high- $Q$  ring cavities (intrinsic  $Q \sim 1$  million provided by low-loss waveguides) with widely-tunable semiconductor lasers to realize narrow-linewidth lasers [91]. Different configurations were studied, including cases where the high- $Q$  cavity is external to the laser cavity and provides filtered optical feedback to the laser cavity and cases where the high- $Q$  cavity is an integral part of the laser cavity (Figure 12).

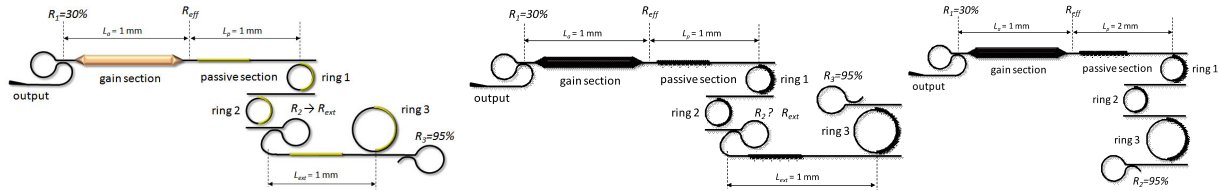


Figure 12. (left) Schematic of external cavity laser with high- $Q$  ring in all-pass configuration (center) Schematic of external cavity laser with high- $Q$  ring in drop configuration (right) Schematic of laser with high- $Q$  ring inside the cavity [91]. Ring 3 is the high- $Q$  ring in all considered cases.

We have studied the three architectures in terms of linewidth performance, by utilizing the theory of adiabatic chirp reduction. For the external high- $Q$  ring cavity lasers, we modify and apply the negative optical feedback theory to estimate the stability of proposed feedback configuration. In terms of stability we show that external high- $Q$  resonator in all-pass configuration provides both higher responsivity and larger  $45^\circ$  phase margin bandwidth (Figure 13).

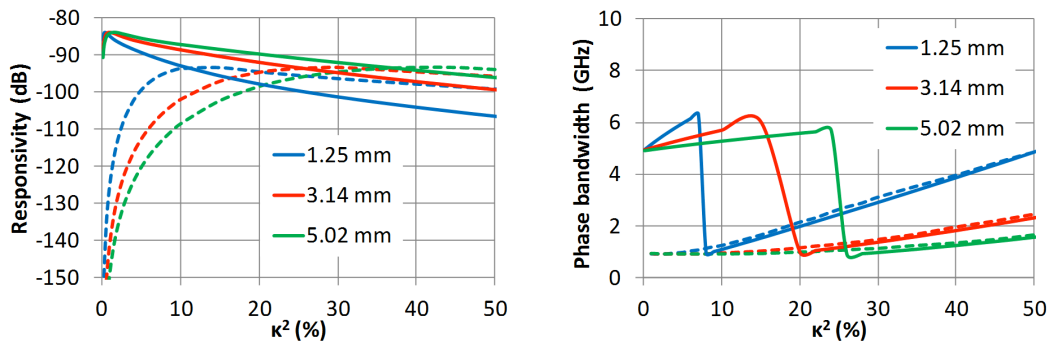


Figure 13. (left) Responsivity of negative optical feedback for various coupling coefficients at low-frequency (10 MHz). All-pass resonator configuration is plotted with full lines, and drop resonator configuration is plotted with dashed lines.. Different colors correspond to different ring resonator circumferences (0.5 dB/cm propagation loss). (right) Phase bandwidth defined for phase margin of  $45^\circ$ . The plot shows frequency where phase surpasses  $135^\circ$  shift, potentially leading to positive feedback and detrimental laser performance (0.5 dB/cm propagation loss, 1 mm loop delay).

Additional analysis showed that although each approach has its advantages and disadvantages, considering all of the aspects of the laser design as well as simplicity of operation, using a high- $Q$  ring as an integral part of the laser cavity is the best approach in order to realize widely-tunable narrow-linewidth monolithically integrated semiconductor lasers. By utilizing heterogeneous integration providing optimized silicon waveguides with low propagation loss, kHz and even sub-kHz instantaneous linewidths should be attainable with proper design (Figure 14).

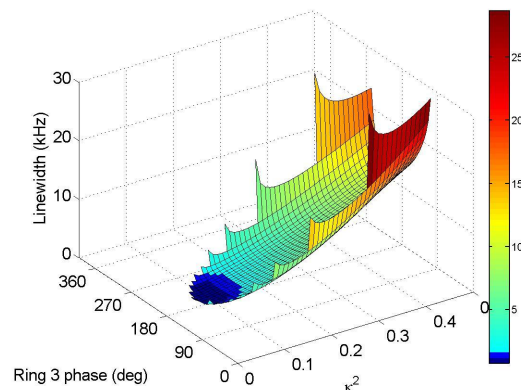


Figure 14. Simulated instantaneous linewidth of laser with high- $Q$  ring inside the cavity as a function of high- $Q$  ring phase and coupling strength (propagation loss 0.5 dB/cm).

## 7. CONCLUSION

Heterogeneous silicon photonics, as it is reaching maturity, becomes attractive not only due to its potential for medium- and large-scale integration and consequently lower cost, but also because it allows for better performance than native III-V devices, as has been recently demonstrated with narrow-linewidth lasers and high-power, high-speed photodiodes.

Furthermore, tight integration of electronics and photonics on-chip allows for better energy efficiency in terms of photonic components and provides a way to avoid interconnect scaling limitation in modern processors.

Heterogeneous silicon photonics may become the technology of choice, not only for future longer range, high speed communications, but also for future data centers, supercomputers, and sensors.

## ACKNOWLEDGMENT

The authors would like to thank B. Koch, G. Fish, E. Norberg, and A. Fang of Aurrion; M. Paniccia, R. Jones, and M. Sysak of Intel; D. Liang, G. Kurczveil and R. Beausoleil of Hewlett Packard; X. Zhang, J. Yao, J. E. Cunningham of Oracle; A. Yariv of Caltech; D. Dai of Zhejiang University; L. Theogarajan, A. Sohdi, L. Chen, D. Blumenthal, L. Coldren, and J. Peters of UCSB for helpful discussions.

## REFERENCES

- [1] J. Bowers, J. Bovington, A. Liu, and A. Gossard, "A Path to 300 mm Heterogeneous Silicon Photonic Integrated Circuits," in *Optical Fiber Communication Conference, OSA Technical Digest (online) (Optical Society of America, 2014)*, paper Th1C.1.
- [2] A. W. Fang, H. Park, R. Jones, O. Cohen, M. J. Paniccia, and J. E. Bowers, "A Continuous Wave Hybrid AlGaInAs-Silicon Evanescent Laser," *IEEE Photonics Technology Letters*, 18 (10), 1143-1145, May 15, 2006
- [3] H. Park, A. W. Fang, S. Kodama, and J. E. Bowers, "Hybrid Silicon Evanescent Laser Fabricated With a Silicon Waveguide and III-V Offset Quantum Wells," *Optics Express*, 13 (23), 9460-9464, November, 2005
- [4] J. E. Bowers, Patents 8,106,379, 8,110,823, 8,937,296, 8,994,004, 9,020,002
- [5] B. Koch, E. Norberg, B. Kim, J. Hutchinson, J. Shin, G. Fish, and A. Fang, "Integrated Silicon Photonic Laser Sources for Telecom and Datacom," in *Optical Fiber Communication Conference/National Fiber Optic Engineers Conference 2013, OSA Technical Digest (online) (Optical Society of America, 2013)*, paper PDP5C.8.
- [6] A. Y. Liu, C. Zhang, J. Norman, A. Snyder, D. Lubyshev, J. M. Fastenau, A. W. K. Liu, A. C. Gossard, and J. E. Bowers, "High performance continuous wave 1.3  $\mu\text{m}$  quantum dot lasers on silicon", *Applied Physics Letters*, 104, 041104 (2014)
- [7] Andrew Lee, Qi Jiang, Mingchu Tang, Alwyn Seeds, and Huiyun Liu, "Continuous-wave InAs/GaAs quantum-dot laser diodes monolithically grown on Si substrate with low threshold current densities," *Opt. Express* 20, 22181-22187 (2012)
- [8] A. Y. Liu, R. W. Herrick, O. Ueda, P. M. Petroff, A. C. Gossard, and J. E. Bowers, "Reliability of InAs/GaAs quantum dot lasers epitaxially grown on silicon," *IEEE Journal of Selected Topics in Quantum Electronics*, Vol 21, No. 6, November/December 2015.
- [9] S. Srinivasan, N. Julian, J. Peters, D. Liang, and J. E. Bowers, "Reliability of Heterogeneous Silicon Distributed Feedback Lasers", *IEEE Journal of Selected Topics In Quantum Electronics*, Vol. 19, No. 4, paper 1501305, July/August 2013
- [10] A. Ramaswamy, J. Roth, E. Norberg, R. S. Guzzon, J. Shin, J. Imamura, B. Koch, D. Sparacin, G. Fish, B. G. Lee, R. Rimolo-Donadio, C. Baks, A. Rylyakov, J. Proesel, M. Meghelli, C. Schow, "A WDM 4x28Gbps Integrated Silicon Photonic Transmitter driven by 32nm CMOS driver ICs", *OFC 2015 post-deadline paper Th5B.5*
- [11] E. Timurdogan, Z. Su, K. Settaluri, S. Lin, S. Moazeni, C. Sun, G. Leake, D. D. Coolbaugh, B. Moss, M. Moresco, V. Stojanovic, M. R. Watts, "An Ultra Low Power 3D Integrated Intra-Chip Silicon Electronic-Photonic Link", *OFC 2015 post-deadline paper Th5B.8*
- [12] K. Takeda, T. Sato, T. Fujii, E. Kuramochi, M. Notomi, K. Hasebe, T. Kakitsuka, and S. Matsuo, "Heterogeneously integrated photonic-crystal lasers on silicon for on/off chip optical interconnects," *Opt. Express* 23, 702-708 (2015)

- [13] R. Kasahara, K. Watanabe, M. Itoh, Y. Inoue and A. Kaneko, "Extremely low power consumption thermo-optic switch (0.6 mW) with suspended ridge and silicon-silica heterogeneous waveguide structures," 34th European Conference on Optical Communication, 2008. ECOC 2008., Sept. 2008
- [14] D. Liang, M. Fiorentino, S. Srinivasan, J. E. Bowers, and R. G. Beausoleil, "Low Threshold Electrically-Pumped Heterogeneous Silicon Microring Lasers", IEEE Journal of Selected Topics in Quantum Electronics, (early access)
- [15] D.A.B. Miller, H.M. Ozaktas, "Limit to the Bit-Rate Capacity of Electrical Interconnects from the Aspect Ratio of the System Architecture", Journal of Parallel and Distributed Computing, Volume 41, Issue 1, 25 February 1997, Pages 42-52, ISSN 0743-7315, <http://dx.doi.org/10.1006/jpdc.1996.1285>.
- [16] C. Batten, A. Joshi, V. Stojanovic, and K. Asanovic, "Designing chip-level nanophotonic interconnection networks," in Integrated Optical Interconnect Architectures for Embedded Systems. New York, NY: Springer, 2013, pp. 81–135
- [17] M. J. R. Heck, J. E. Bowers, "Energy Efficient and Energy Proportional Optical Interconnects for Multi-Core Processors: Driving the Need for On-Chip Sources", IEEE Journal of Selected Topics In Quantum Electronics, Vol. 20, No. 4, July/August 2014.
- [18] R. Ho, P. Amberg, E. Chang, P. Koka, J. Lexau, G. Li, F. Y. Liu, H. Schwetman, I. Shubin, H. D. Thacker, X. Zheng, J. E. Cunningham, and A. V. Krishnamoorthy, "Silicon photonic interconnects for large-scale computer systems," IEEE Micro, vol. 33, no. 1, pp. 68–78, Jan./Feb. 2013.
- [19] J. Miller, J. Psota, G. Kurian, N. Beckmann, J. Eastep, J. Liu, M. Beals, J. Michel, L. Kimerling, and A. Agarwal, "ATAC: A manycore processor with on-chip optical network," Massachusetts Institute of Technology, Cambridge, MA, USA, MIT-CSAIL-TR-2009-018, May 5, 2009.
- [20] L. Chen, A. Sohdi, J. E. Bowers, L. Theogarajan, J. Roth and G. Fish, "Electronic and Photonic Integrated Circuits for Fast Data Center Optical Circuit Switches", IEEE Communications Magazine, Vol. 51, No. 9, pp. 53 – 59, September 2013
- [21] P. Rabiei, J. Ma, S. Khan, J. Chiles, and S. Fathpour, "Heterogeneous lithium niobate photonics on silicon substrates", Optics Express, Vol. 21, No. 21, pp. 25573-25581, DOI:10.1364/OE.21.025573 21 October 2013
- [22] L. Chen, Q. Xu, M. G. Wood, and R. M. Reano, "Heterogeneous silicon and lithium niobate electro-optical ring modulator", Optica, vol. 1, no. 2, pp. 112-118, August 2014
- [23] M.-C. Tien, T. Mizumoto, P. Pintus, H. Kromer, and J. E. Bowers, "Silicon ring isolators with bonded nonreciprocal magneto-optic garnets," Optics Express 19, 11740-11745 (2011)
- [24] L. Bi, J. Hu, P. Jiang, D. H. Kim, G. F. Dionne, L. C. Kimerling, and C. A. Ross, "On-chip optical isolation in monolithically integrated non-reciprocal optical resonators", Nature Photonics 5, pp. 758–762 (2011) doi:10.1038/nphoton.2011.270
- [25] Y. Shoji and T. Mizumoto, "Magneto-optical non-reciprocal devices in silicon photonics", Science and Technology of Advanced Materials, Vol. 15, No. 1, paper 014602, doi:10.1088/1468-6996/15/1/014602
- [26] P. Rojo-Romeo, J. Van Campenhout, F. Mandorlo, C. Seassal, X. Letratre, P. Regreny, D. Van Thourhout, R. Baets, L. Di Cioccio, and J. Fedeli, "Integration of an Electrically Driven InGaAsP Based Microdisk Laser with a Silicon Based Passive Photonic Circuit," in Conference on Lasers and Electro-Optics/Quantum Electronics and Laser Science Conference and Photonic Applications Systems Technologies, OSA Technical Digest Series (CD) (Optical Society of America, 2007), paper CWN1.
- [27] K. Bergman, "Silicon Photonic On-Chip Optical Interconnection Networks", The 20th Annual Meeting of the IEEE Lasers and Electro-Optics Society, 2007. - LEOS 2007. , pp.470-471, 21-25 Oct. 2007
- [28] L. Chen, J. Chen, J. Nagy, and R. M. Reano, "Highly linear ring modulator from hybrid silicon and lithium niobate," Opt. Express 23, 13255-13264 (2015)
- [29] M. J. R. Heck, J. F. Bauters, M. Davenport, J. K. Doylend, S. Jain, G. Kurezveil, S. Srinivasan, Y. Tang, and J. E. Bowers, "Heterogeneous Silicon Photonic Integrated Circuit Technology", IEEE Journal of Selected Topics In Quantum Electronics, Vol. 19, No. 4, July/August 2013, paper 6100117
- [30] F. Xia, L. Sekaric, and Y. Vlasov, "Ultracompact optical buffers on a silicon chip", Nature Photonics 1, 65 - 71 (2007) , doi:10.1038/nphoton.2006.42
- [31] S. Srinivasan, M. Davenport, T. Komljenovic, J. Hulme, D. T. Spencer, J. E. Bowers, "Coupled Ring Resonator Mirror Based Heterogeneous III-V Silicon Tunable Laser", IEEE Photonics Journal, doi:10.1109/JPHOT.2015.2428255
- [32] D. Dai and J. E. Bowers, "Silicon-based on-chip multiplexing technologies and devices for Peta-bit optical interconnects"; Nanophotonics; pp: 1–30; DOI: 10.1515/nanoph-2013-0021; 14 November 2014

- [33] Y. Vlasov and S. McNab, "Losses in single-mode silicon-on-insulator strip waveguides and bends," *Opt. Express* 12, 1622-1631 (2004)
- [34] A. Biberman, M. Shaw, E. Timurdogan, J. Wright, and M. Watts, "Ultralow-loss silicon ring resonators," *Opt. Lett.* 37, 4236-4238 (2012).
- [35] N. Kobayashi, K. Sato, M. Namiwaka, K. Yamamoto, S. Watanabe, T. Kita, H. Yamada, H. Yamazaki, "Silicon Photonic Heterogeneous Ring-Filter External Cavity Wavelength Tunable Lasers," *Journal of Lightwave Technology*, vol. 33, no. 6, pp. 1241-1246, March, 15 2015.
- [36] T. Komljenovic, S. Srinivasan, E. Norberg, M. Davenport, G. Fish, J. E. Bowers, "Widely-tunable narrow-linewidth monolithically-integrated external-cavity semiconductor lasers", *IEEE Journal of Selected Topics in Quantum Electronics* (early access)
- [37] J. F. Bauters, M. J. R. Heck, D. D. John, J. S. Barton, C. M. Bruinink, A. Leinse, R. G. Heideman, D. J. Blumenthal, and J. E. Bowers, "Planar waveguides with less than 0.1 dB/m propagation loss fabricated with wafer bonding," *Opt. Express* 19, 24090-24101 (2011)
- [38] J. F. Bauters, M. L. Davenport, M. J. R. Heck, J. K. Doylend, A. Chen, A. W. Fang, and J. E. Bowers, "Silicon on ultra-low-loss waveguide photonic integration platform," *Opt. Express* 21, 544-555 (2013)
- [39] E. J. Stanton, M. J. R. Heck, J. Bovington, A. Spott, and J. E. Bowers, "Multi-octave spectral beam combiner on ultrabroadband photonic integrated circuit platform", *Optics Express*, Vol. 23, No. 9, pp. 11272-11283, 4 May 2015, DOI:10.1364/OE.23.011272
- [40] D. Dai, Z. Wang, and J. Bowers, "Ultrashort broadband polarization beam splitter based on an asymmetrical directional coupler," *Opt. Lett.* 36, 2590-2592 (2011).
- [41] D. Dai and J. Bowers, "Novel ultra-short and ultra-broadband polarization beam splitter based on a bent directional coupler," *Opt. Express* 19, 18614-18620 (2011).
- [42] J. Wang, D. Liang, Y. Tang, D. Dai, and J. Bowers, "Realization of an ultra-short silicon polarization beam splitter with an asymmetrical bent directional coupler," *Opt. Lett.* 38, 4-6 (2013).
- [43] Z. Wang, D. Dai, "Ultras-small Si-nanowire-based polarization rotator", *J. Opt. Soc. Am. B* 25, p. 747, 2008.
- [44] D. Vermeulen, S. Selvaraja, P. Verheyen, P. Absil, W. Bogaerts, D. Van Thourhout, G. Roelkens, Silicon-on-insulator polarization rotator based on a symmetry breaking silicon overlay, *IEEE Photon. Technol. Lett.* 24, p. 482, 2012.
- [45] D. Dai and J. Bowers, "Novel concept for ultracompact polarization splitter-rotator based on silicon nanowires," *Opt. Express* 19, 10940-10949 (2011).
- [46] Bradley J. Frey, Douglas B. Leviton, Timothy J. Madison, "Temperature-dependent refractive index of silicon and germanium", *Proc. SPIE* 6273, *Optomechanical Technologies for Astronomy*, 62732J (July 06, 2006); doi:10.1117/12.672850.
- [47] G. Coppola, L. Sirleto, I. Rendina, M. Iodice, "Advance in thermo-optical switches: principles, materials, design, and device structure" *Optical Engineering*, Vol. 50, no. 7, . paper 071112 May, 2011.
- [48] T. Barwicz; M. A. Popovic; F. Gan; M. S. Dahlem; C. W. Holzwarth; P. T. Rakich; E. P. Ippen; F. X. Kärtner; H. I. Smith, "Reconfigurable silicon photonic circuits for telecommunication applications", *Proc. SPIE* 6872, *Laser Resonators and Beam Control X*, 68720Z (7 February 2008); doi: 10.1117/12.772740
- [49] J. Bovington, S. Srinivasan, and J. E. Bowers, "Athermal laser design", *Optics Express*, Vol. 22, No. 16, pp. 19357-19364, 11 August 2014, DOI:10.1364/OE.22.019357
- [50] S. Feng, K. Shang, J. T. Bovington, R. Wu, K-T. Cheng, , J. E. Bowers, and S.J.B. Yool "Athermal Characteristics of TiO<sub>2</sub>-Clad Silicon Waveguides at 1.3 $\mu$ m", 2014 IEEE Photonics Conference (IPC), pp. 116 – 117, San Diego, CA
- [51] J. Bovington, R. Wu, K.-T. Cheng, and J. E. Bowers, "Thermal stress implications in athermal TiO<sub>2</sub> waveguides on a silicon substrate", *Optics Express*, Vol. 22, No. 1, pp. 661-666, 13 January 2014, DOI:10.1364/OE.22.000661
- [52] H. Tanobe, Y. Kondo, Y. Kadota, K. Okamoto, and Y. Yoshikuni, "Temperature insensitive arrayed waveguide gratings on InP substrates," *IEEE Photon. Technol. Lett.* 10(2), 235–237 (1998).
- [53] V. Raghunathan, W. N. Ye, J. Hu, T. Izuhara, J. Michel, and L. Kimerling, "Athermal operation of Silicon waveguides: spectral, second order and footprint dependencies", *Optics Express* 18, 17631-17639 (2010).
- [54] A. W. Fang, H. Park, O. Cohen, R. Jones, M. J. Paniccia, and J.E. Bowers, "Electrically pumped heterogeneous AlGaInAs-silicon evanescent laser," *Opt. Exp.*, vol. 14, pp. 9203–9210, 2006.
- [55] A. De Groote, J. D. Peters, M. L. Davenport, M. J. R. Heck, R. Baets, G. Roelkens, and J. E. Bowers, "Heterogeneously integrated III–V-on-silicon multibandgap superluminescent light-emitting diode with 290 nm optical bandwidth," *Opt. Lett.* 39, 4784-4787 (2014)

- [56] S. Srinivasan, E. Norberg, T. Komljenovic, M. Davenport, G. Fish, and J. E. Bowers, "Heterogeneous Silicon Colliding-Pulse Mode-Locked-Lasers with On-Chip Stabilization", *IEEE Journal of Selected Topics in Quantum Electronics*, (early access)
- [57] C. Zhang, S. Srinivasan, Y. Tang, M. J. R. Heck, M. L. Davenport, and J. E. Bowers, "Low threshold and high speed short cavity distributed feedback heterogeneous silicon lasers", *Optics Express*, Vol. 22, No. 9, pp. 10202 - 10209, 5 May 2014, DOI:10.1364/OE.22.010202
- [58] C. Zhang, D. Liang, G. Kurczveil, J. E. Bowers, and R. G. Beausoleil, "Thermal Management of Hybrid Silicon Ring Lasers for High Temperature Operation", *IEEE Journal of Selected Topics in Quantum Electronics*, (early access)
- [59] H. D. Thacker, Y. Luo, J. Shi, I. Shubin, J. Lexau, X. Zheng, G. Li, J. Yao, J. Costa, T. Pinguet, A. Mekis, P. Dong, S. Liao, D. Feng, M. Asghari, R. Ho, K. Raj, J. G. Mitchell, A. V. Krishnamoorthy and J. E. Cunningham, "Flip-Chip Integrated Silicon Photonic Bridge Chips for Sub-Picojoule Per Bit Optical Links", *Electronic Components and Technology Conference (ECTC), 2010 Proceedings 60th*, pp 240-246 (2010)
- [60] R. F. Kazarinov, C. H. Henry, "The relation of line narrowing and chirp reduction resulting from the coupling of a semiconductor laser to passive resonator," *IEEE Journal of Quantum Electronics*, vol. 23, no. 9, pp. 1401 - 1409, Sep. 1987.
- [61] X. Xie, Q. Zhou, E. Norberg, M. Jacob-Mitos, Y. Chen, A. Ramaswamy, G. Fish, J. E. Bowers, J. Campbell, and A. Belling, "Heterogeneously Integrated Waveguide-Coupled Photodiodes on SOI with 12 dBm Output Power at 40 GHz," *OFC 2015 post-deadline paper Th5B.7*
- [62] S. Srinivasan, R. Moreira, D. Blumenthal and J. E. Bowers, "Design of integrated heterogeneous silicon waveguide optical gyroscope", *Optics Express*, Volume: 22 Issue: 21 Pages: 24988 DOI:10.1364/OE.22.024988, October 20, (2014)
- [63] S. Srinivasan, J. E. Bowers, "Integrated High Sensitivity Heterogeneous Silicon Magnetometer", *IEEE Photonics Technology Letters*, Volume: 26, Issue:13, 1 July, (2014)
- [64] A. Spott, M. Davenport, J. Peters, J. Bovington, M. J. R. Heck, E. J. Stanton, I. Vurgaftman, J. Meyer, J. E. Bowers, "Heterogeneously integrated 2.0  $\mu\text{m}$  CW heterogeneous silicon lasers at room temperature", *Optics Letters*, vol 40 (7) p. 1480, April 1, (2015)
- [65] J. C. Hulme, J. K. Doyle, M. J. R. Heck, J. D. Peters, M. L. Davenport, J. T. Bovington, L. A. Coldren, and J. E. Bowers, "Fully integrated heterogeneous silicon two dimensional beam scanner", *Optics Express*, Vol. 23, No. 5, pp. 5861-5874, 9 Mar 2015, DOI:10.1364/OE.23.005861
- [66] A. Y. Liu, C. Zhang, A. Snyder, D. Lubyshev, J. M. Fastenau, A. W. K. Liu, A. C. Gossard, and J. E. Bowers, "MBE growth of P-doped 1.3  $\mu\text{m}$  quantum dot lasers on silicon", *Journal of Vacuum Science & Technology B*, 32, 02C108 (2014)
- [67] M. Seimetz, "Laser Linewidth Limitations for Optical Systems with High-Order Modulation Employing Feed Forward Digital Carrier Phase Estimation", *OFC 2008*, paper OTuM2
- [68] M. Larson, Y. Feng, P. Koh, X. Huang, M. Moewe, A. Semakov, A. Patwardhan, E. Chiu, A. Bhardwaj, K. Chan, J. Lu, S. Bajwa, and K. Duncan, "Narrow linewidth high power thermally tuned sampled-grating distributed Bragg reflector laser," in *Optical Fiber Communication Conference/National Fiber Optic Engineers Conference 2013*, OSA Technical Digest (online) (Optical Society of America, 2013), paper OTh31.4.
- [69] M. Larson, A. Bhardwaj, W. Xiong, Y. Feng, X. Huang, K. Petrov, M. Moewe, H. Ji, A. Semakov, C. Lv, S. Kutty, A. Patwardhan, N. Liu, Z. Li, Y. Bao, Z. Shen, S. Bajwa, F. Zhou, and P. Koh, "Narrow linewidth sampled-grating distributed Bragg reflector laser with enhanced side-mode suppression," in *Optical Fiber Communication Conference*, OSA Technical Digest (online) (Optical Society of America, 2015), paper M2D.1.
- [70] H. Ishii, K. Kasaya, and H. Oohashi, "Spectral Linewidth Reduction in Widely Wavelength Tunable DFB Laser Array," *IEEE Jour. Of Select. Top. In Quant. Electron.*, vol. 15, no. 3, May-Jun 2009.
- [71] G. W. Yoffe et al., "Widely-tunable 30mW laser source with sub-500kHz linewidth using DFB array," *21st Annual Meeting of the IEEE Lasers and Electro-Optics Society*, 2008. LEOS 2008., pp. 892 - 893, Nov. 2008.
- [72] H. Ishii, K. Kasaya and H. Oohashi, "Narrow spectral linewidth operation (<160 khz) in widely tunable distributed feedback laser array," *Electron. Letters*, vol. 46, no. 10, pp. 714 - 715, May 2010.
- [73] Y. Sasahata et al., "Tunable 16 DFB Laser Array with Unequally Spaced Passive Waveguides for Backside Wavelength Monitor," in *Optical Fiber Communications Conference and Exhibition 2014 (OFC2014)*, paper Th3A.2., Mar. 2014.
- [74] H. Ishii et al., "Narrow spectral linewidth under wavelength tuning in thermally tunable super-structure-grating (SSG) DBR lasers," *IEEE Jour. Of Select. Top. In Quant. Electron.*, vol. 1, no. 2, pp. 401 - 407, Jun 1995.

- [75] N. Kobayashi et al., "Silicon Photonic Heterogeneous Ring-Filter External Cavity Wavelength Tunable Lasers," *IEEE Journ. of Lightw. Tech.*, vol. 33, no. 6, pp. 1241-1246, Mar. 2015
- [76] T. Creazzo et al., "Integrated tunable CMOS laser," *Opt. Express*, vol. 21, no. 23, pp. 28048-28053, Nov. 2013.
- [77] T. Matsumoto et al., "Narrow Spectral Linewidth Full Band Tunable Laser Based on Waveguide Ring Resonators with Low Power Consumption," in *Optical Fiber Communication Conference 2010*, OSA Technical Digest (CD) (Optical Society of America, 2010), paper OThQ5.
- [78] J. Hulme, J. Doyle, and J. Bowers, "Widely tunable Vernier ring laser on heterogeneous silicon," *Opt. Express*, vol. 21, no. 17, pp. 19718-19722, Aug. 2013.
- [79] T. Komljenovic, M. Davenport, S. Srinivasan, J. Hulme, and J. E. Bowers, "Narrow linewidth tunable laser using coupled resonator mirrors," in *Optical Fiber Communication Conference*, OSA Technical Digest (online) (Optical Society of America, 2015), paper W2A.52.
- [80] S. Keyvaninia, G. Roelkens, D. Van Thourhout, C. Jany, M. Lamponi, A. Le Liepvre, F. Lelarge, D. Make, G.-H. Duan, D. Bordel, and J.-M. Fedeli, "Demonstration of a heterogeneously integrated III-V/SOI single wavelength tunable laser," *Opt. Express* 21, 3784-3792 (2013)
- [81] K. Nemoto, T. Kita and H. Yamada, "Narrow-Spectral-Linewidth Wavelength-Tunable Laser Diode with Si Wire Waveguide Ring Resonators," *Appl. Phys. Express*, vol. 5, 082701, Aug. 2012.
- [82] T. Kita, K. Nemoto, and H. Yamada, "Long external cavity Si photonic wavelength tunable laser diode," *Jpn. J. Appl. Phys.*, vol. 53, 04EG04, Feb. 2014.
- [83] C. T. Santis, S. T. Steger, Y. Vilenchik, A. Vasilyev, and A. Yariv, "High-coherence semiconductor lasers based on integral high-Q resonators in heterogeneous Si/III-V platforms", *PNAS* 2014 111 (8) 2879-2884; February 10, 2014, doi:10.1073/pnas.1400184111
- [84] C. T. Santis, and A. Yariv, "High-Q Silicon Resonators For High-Coherence Heterogeneous Si/III-V Semiconductor Lasers", *CLEO 2015 paper*, SW3F.5.pdf
- [85] C. T. Santis, Y. Vilenchik, A. Yariv, N. Satyan, and G. Rakuljic, "Sub-kHz Quantum Linewidth Semiconductor Laser On Silicon Chip", *CLEO 2015 post-deadline paper*, JTh5A.7.pdf
- [86] B. Liu, A. Shakouri and J. E. Bowers, "Passive microring-resonator-coupled lasers", *Appl. Phys. Lett.* 79, 3561 (2001); <http://dx.doi.org/10.1063/1.1420585>
- [87] B. Liu, A. Shakouri, and J. E. Bowers, "Wide Tunable Double Ring Resonator Coupled Lasers", *IEEE Photonics Technology Letters*, Vol. 14, No. 5, pp. 600-602, May 2002
- [88] D. Miller, "Device requirements for optical interconnects to silicon chips," *Proc. IEEE*, vol. 97, no. 7, pp. 1166-1185, Jul. 2009.
- [89] L. Agazzi, J. D. B. Bradley, M. Dijkstra, F. Ay, G. Roelkens, R. Baets, K. Wörhoff, and M. Pollnau, "Monolithic integration of erbium-doped amplifiers with silicon-on-insulator waveguides," *Opt. Express* 18, 27703-27711 (2010)
- [90] S. Koeber, R. Palmer, M. Lauer, W. Heni, D. L. Elder, D. Korn, M. Woessner, L. Alloatti, S. Koenig, P. C. Schindler, H. Yu, W. Bogaerts, L. R. Dalton, W. Freude, J. Leuthold, and C. Koos "Femtojoule electro-optic modulation using a silicon-organic hybrid device", *Light: Science & Applications* (2015) 4, e255; doi:10.1038/lsa.2015.28
- [91] T. Komljenovic, J. E. Bowers, "Monolithically-Integrated High-Q Rings for Narrow-Linewidth Widely-Tunable Lasers," *IEEE Journal of Quantum Electronics*, vol. 51, no. 11, Article# 0600610, Nov. 2015.